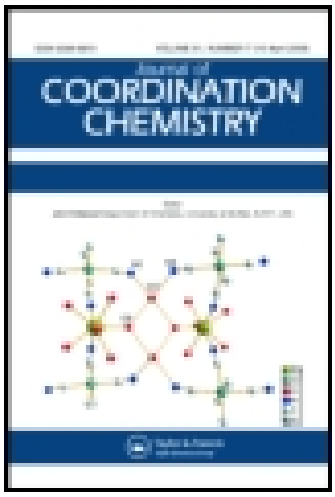

Journal of Coordination Chemistry
Publication details, including instructions for authors and subscription information:
http://www.tandfonline.com/loi/gcoo20

Aliphatic polyamine ruthenium(II) complexes: Crystal structure, DNA-binding, photocleavage, cytotoxicity and antioxidation

Xian-Lan Hong[a] & Wen-Guan Lu[a]
[a] Department of Chemistry, Shaoguan University, Shaoguan, Guangdong, 512005, PR China
Accepted author version posted online: 01 Sep 2015.

Publisher: Taylor & Francis
Journal: *Journal of Coordination Chemistry*
DOI: http://dx.doi.org/10.1080/00958972.2015.1088527

Aliphatic polyamine ruthenium(II) complexes: Crystal structure, DNA-binding, photocleavage, cytotoxicity and antioxidation

XIAN-LAN HONG* and WEN-GUAN LU*

Department of Chemistry, Shaoguan University, Shaoguan, Guangdong, 512005, PR China

The DNA-binding behaviors of two aliphatic polyamine Ru(II) complexes, $[Ru(dppt)(dien)](ClO_4)_2$ (**1**) and $[Ru(pta)(dien)](ClO_4)_2$ (**2**) (dppt, pta and dien standing for 3-(1,10-phenanthrolin-2-yl)-5,6-diphenyl-as-triazine, 3-(1,10-phenanthrolin-2-yl)-5,6-diphenyl-as-triazino[5,6-f]-acenaphthylene and diethylenetriamine, respectively), were studied through absorption titration, thermal denaturation and viscosity measurements. The results indicate that the DNA-binding affinity of **2** is much greater than that of **1**; **2** binds to CT-DNA in an intercalative mode but **1** binds to CT-DNA through partial intercalation. In addition, the complexes react with DNA in an energy-driven process with a decrease of entropy. The photocleavage of plasmid pBR322 can be triggered by **1** and **2** and strengthened with an increased concentration of both complexes. The scavenging activity of **1** against hydroxyl radical (•OH) is slightly better than that of **2** according to the antioxidation experiment. The standard cytotoxicity experiments were carried out with MTT (3-(4,5-dimethylthiazol-2-yl)-2,5-diphenyltetrazolium bromide); the results indicate that the proliferation of Hela, A549 and 7402 cells is inhibited by these two compounds in a dose-dependent manner. The X-ray crystal structure of **1** and some results of DFT (the density functional theory) calculations were analyzed to further understand the differences in DNA-binding strength of the complexes.

Keywords: Ruthenium complex; aliphatic polyamine; DNA-Binding; cytotoxicity; antioxidation

*Corresponding authors. Email: hongxianlan@163.com (X.L. Hong); luwenguan@aliyun.com (W.G. Lu)

1. Introduction

Substitutionally inert, photo-chemical, photo-physical and redox properties allow coordinatively saturated polypyridyl ruthenium(II) complexes to have applications in biologically active agents like DNA-reactants [1-6], antioxidants [7] and anticarcinogens [8-14]. Studies on these compounds have expanded in fields ranging from nucleic acid chemistry to cellular biology, and the main research content includes the two following areas: (1) synthesizing serial heteroaromatic compounds with special fragments, such as pyrazine [3, 8, 12], 1,2,4-triazine [2i], 5,6-dihydrouracil [2h], 1,4-cyclohexanedione [11], and various functional groups including halogen [7a, 7e], nitryl [2b, 2g, 10, 13], amino [7b-d] and methoxyl [2g, 10, 13], which can be used as main ligands, together with bpy or phen derivatives as ancillary ligands (co-ligands), to construct various Ru(II) complexes; (2) exploring the effect of both the main ligand and ancillary ligand on biological activities of the overall complexes, such as the mode or strength of DNA-binding, cellular uptake, cytotoxicity and oxidation resistance. We note that there is growing interest in the relationship of the bioactivities of the complexes and co-ligands on their respective properties, such as volume size, coplanarity, lipophilicity, and coordinative stereo-hindrance. A combination of better coplanarity with better lipophilicity of the ancillary ligand is generally beneficial to DNA-binding of the complex [2h, 7d], cellular uptake and anti-proliferation activity against cancer cells [2j, 11, 14]. However, in some cases, especially for the tridentate complexes, only increasing the size of the ancillary ligand to add lipophilicity can decrease the DNA-binding and other bioactivities to some extent [3, 7e, 12, 15]. Complexes with bulky co-ligands and better lipophilicity have greater ease in cellular uptake, but seem to not readily enter the cell nuclei to target DNA. Strategies for changing the co-ligand to enhance bioactivity have been reported, such as introducing electropositive pendants [2e] or forming a Ru-C covalent bond; more importantly, the latter can cause the resulting complex to not only have greater ease in cellular uptake but also to more easily penetrate the cellular karyotheca because of the increasing lipophilicity without any increasing size in the overall complex [2j]. Most of the reported complexes, similar to cisplatin analogs [16], are less soluble in

water due to their large heteroaromatic hydrophobic ligands, and thus their applications as anticancer drugs are limited [2d]. Ru(II) complexes containing ammonia [17, 18], amine [19, 20] and imidazole [2d] as ancillary ligands are very soluble in water, and our research stems from interest in designing and synthesizing water soluble aliphatic polyamine Ru(II) complexes. Two series of Ru(II) complexes containing dipn (N-(3-aminopropyl)-1,3-propanediamine) and dien were synthesized and characterized [19, 20] (the DNA-binding properties of dipn-containing ruthenium complexes were also studied in previous work [19]). DNA-binding strength of dipn complexes is smaller than that of related tpy complexes because of the H-bonding between the N-H of the co-ligand and the N or O atom the bases of the sugar-phosphate backbone of DNA, similar to the order of DNA-binding strength: $[Ru(phen)_2dppz]^{2+}$ > $[Ru(NH_3)_4dppz]^{2+}$ [17]. As a part of our systematic studies, in this contribution we have further explored the DNA-binding properties of two dien-containing complexes, $[Ru(dppt)(dien)]^{2+}$ (**1**) and $[Ru(pta)(dien)]^{2+}$ (**2**), for discussing the effect of features of co-ligand aliphatic polyamine on DNA-binding properties. Meanwhile, the antioxidation and cancer cell cytotoxicity of **1** and **2** were also investigated.

2. Experimental

2.1. *General*

$[Ru(dppt)(dien)]^{2+}$ (**1**) and $[Ru(pta)(dien)]^{2+}$ (**2**) were synthesized according to literature methods [20] and all the aqueous solutions were prepared with doubly distilled water. Calf thymus DNA (Sigma Chemical Co.), pBR 322 DNA (Shanghai Sangon Biological Engineering & Services Co.), agarose, ethidium bromide (EB) (Aldrich), and other chemicals were commercially available. The buffers were prepared with the following compositions: A (5 mM Tris-HCl, 50 mM NaCl, pH 7.0), B (1.5 mM Na_2HPO_4, 0.5 mM NaH_2PO_4, 0.25 mM Na_2EDTA, pH 7.0), C (50 mM Tris-HAc, 18 mM NaCl, pH 7.2), and D (50% DMF, 20% sodium dodecyl sulfate). Calf thymus DNA solutions gave a ratio of UV absorbance at 260 and 280 nm of *ca.* 1.8-1.9:1, indicating that the DNA was sufficiently free of protein [21]. The DNA concentration per nucleotide was determined with the spectrophotometric method by assuming ε_{260} = 6600 M^{-1} cm^{-1} at 260 nm [22].

2.2. *X-ray crystallography*

The crystal of **1**, suitable for X-ray single crystal analysis, was obtained through slow evaporation of acetonitrile-toluene (1:1, v/v) solution at ambient temperature. Diffraction data were collected on a Bruker Smart 1000 CCD diffractometer equipped with graphite monochromated Mo-Kα radiation (λ = 0.71073 Å) at 100 K. Absorption corrections for **1** were applied by SADABS [23]. The structure was solved by direct methods and refined using full-matrix least-squares/difference Fourier techniques using SHELXTL [24, 25]. All hydrogens of the ligands were placed at idealized positions and refined as riding with the relative isotropic parameters of the heavy atoms to which they were attached; all non-hydrogen atoms were refined with anisotropic displacement parameters. Crystallographic data for the structure reported here has been deposited in the Cambridge Crystallographic Data Center (CCDC), No. CCDC 943190; Email: deposit@ccdc.cam.ac.uk.

2.3. *CT-DNA binding and pBR-DNA cleavage*

Absorption titration at room temperature was carried out using a 3 ml solution of **1** or **2** (20 μM, buffer A) to which increments of the DNA stock solution were added until it reached a 10:1 ratio of [DNA]:[Ru]. The Ru(II)-DNA solutions were allowed to incubate for 5 min before absorption spectra were recorded. The intrinsic DNA-binding constant K_{b1} for the two complexes was fitted by the following equations based on a more realistic site-exclusion model [26]:

$$(\varepsilon_a - \varepsilon_f)/(\varepsilon_b - \varepsilon_f) = (b - (b^2 - 2K_{b1}^2 C_1[\mathrm{DNA}]/s)^{1/2})/2K_{b1}C_1 \quad (1a)$$

$$b = 1 + K_{b1}C_1 + K_{b1}[\mathrm{DNA}]/2s \quad (1b)$$

where [DNA] is the concentration of DNA in base pairs and ε_a, ε_f and ε_b correspond to the apparent absorption coefficient $A_{obsd}/[\mathrm{Ru}]$, the extinction coefficient for the free ruthenium complex, and the extinction coefficient for the ruthenium complex in the fully bound form, respectively, C_1 is the

total metal complex concentration, and *s* is the number of binding base pairs occupied by each molecule of **1** or **2**.

The UV DNA melting experiment was performed with a Perkin-Elmer Lambda 35 spectrophotometer equipped with a Peltier temperature-controlling programmer (± 0.1 °C). The melting curves were obtained by measuring the absorbance at 260 nm for solutions of CT-DNA (100 μM, buffer B) in the absence and presence of the Ru(II) complex (10 μM) as a function of temperature. The temperature of the solution was increased by 1 °C min^{-1} and ramped up from 50 to 90 °C. The data were presented as $(A - A_0)/(A_f - A_0)$ versus temperature, where A, A_0, and A_f represent the observed, the initial, and the final absorbance at 260 nm, respectively.

The DNA binding constant K_{b2} of the complex at T_m was obtained with Eq. 2 [27]:

$$\frac{1}{T_m^0} - \frac{1}{T_m} = (\frac{R}{\Delta H_m}) \ln(1 + K_{b2} C_2)^{1/s} \qquad (2)$$

T_m^0 and T_m are the melting temperatures of CT-DNA alone and in the presence of the complex, respectively. ΔH_m is the enthalpy of DNA (per base pair), the value 28.9 kJ·mol^{-1} was determined by differential scanning calorimetry [28a], R is the gas constant, C_2 is the free Ru(II) complex concentration (10 μM here), and s is as it was in Eq. 1.

According to van't Hoffs Eqs. 3-5 [29], a series of thermodynamic functions can be calculated:

$$\ln\left(\frac{K_{b2}}{K_{b1}}\right) = \frac{\Delta H^0}{R}\left(\frac{1}{T} - \frac{1}{T_m}\right) \qquad (3)$$

$$\Delta G^0 = -RT \ln K_{b1} \qquad (4)$$

$$\Delta G^0 = \Delta H^0 - T\Delta S^0 \qquad (5)$$

Journal of Coordination Chemistry

K_{b1} and K_{b2} are as they were in Eqs. 1 and 2; ΔH^0, ΔG^0 and ΔS^0 are the DNA-binding changes in standard enthalpy, standard free energy, and the standard entropy of the complex, respectively.

The viscosity measurements of DNA solution in buffer A were performed following the literature method [30]. The measuring flow time with the Ubbelodhe viscometer was processed into the relative viscosity η, and the data were presented as $(\eta/\eta^0)^{1/3}$ versus the binding ratio of [Ru] to [DNA], η^0 and η here are the viscosity of DNA in the presence and absence of the complex, respectively [31].

Super-coiled pBR322 DNA (0.1 μg) in the gel electrophoresis experiment was treated with the Ru(II) solution of buffer C, then irradiated at room temperature with a UV lamp (365 nm, 10 W). Samples were analyzed by eletrophoresis for 1 h at 100 V on a 0.8% agarose gel in TBE (89 mM Tris-borate acid, 2 mM EDTA, pH = 8.3). The gel was stained with 1 μg/ml ethidium bromide and photographed on an Alpha Innotech IS–5500 fluorescence chemiluminescence and visible imaging system.

2.4. *Antioxidation experiment: scavenger measurements of hydroxyl radical (•OH)*

The hydroxyl radical (•OH) in aqueous media was generated by Fenton's reagent [32]. The solutions of **1** and **2** were prepared with N,N-dimethylformamide (DMF) and 5 ml of an assay mixture of safranin (28.5 μM); EDTA-Fe(II) (100 μM), H_2O_2 (44.0 μM), Ru(II) (0.5-10.0 μM) and a phosphate buffer (67 mM, pH = 7.4) were prepared according to the literature method [33]. The assay mixtures were incubated at 37 °C for 30 min in a water bath and the absorbance was then measured at 520 nm. All the tests were run in triplicate and expressed as the mean. The scavenging ratio (η_a) was calculated using Eq. 6:

$$\eta_a = (A_i - A_0)/(A_c - A_0) \qquad (6)$$

where A_i was the absorbance in the presence of the tested compound, A_0 was the absorbance in the absence of the tested compound, and A_c was the absorbance in the absence of the tested compound, EDTA-Fe(II), and H_2O_2.

2.5. *Cell viability assay*

Standard 3-(4,5-dimethylthiazole)-2,5-diphenyltetraazolium bromide (MTT) assay procedures were used for cytotoxicity [34]. Cells were seeded in 96-well microassay culture plates (2×10^4 cells per well) and incubated overnight at 37 °C in a 5% CO_2 incubator. Tested compounds were dissolved in DMSO and diluted with RPMI 1640 to the required concentrations prior to use. Control wells were prepared by addition of culture medium (100 μL). Wells containing culture medium without cells were used as blanks. The plates were incubated at 37 °C in a 5% CO_2 incubator for 48 h. Upon completion of the incubation, stock MTT dye solution (20 μL, 5 mg mL^{-1}) was added to each well. After 4 h of incubation, a buffer (100 μL) containing DMF (50%) and sodium dodecyl sulfate (20%) was added to solubilize the MTT formazan. The optical density of each well was then measured on a microplate spectrophotometer at a wavelength of 490 nm. The IC_{50} values were determined by plotting the percentage viability versus concentration on a logarithmic graph and reading off the concentration at which 50% of cells remained viable relative to the control. Each experiment was repeated at least three times to get the mean values. Three tumor cell lines, BEL-7402 (hepatocellular), A549 (human pulmonary carcinoma), and HELA (human cervical carcinoma), were purchased from American Type Culture Collection, Beijing, China.

3. Results and discussion

3.1. *Crystal structure of 1*

The collected data and refinement details for the single crystal of **1** and selected bond lengths and angles were given in tables 1 and 2, respectively. According to figure 1 and the data in table 2, the Ru(II) is coordinated by six nitrogens from dppt (N_1, N_{14} and N_{20}) and dien (N_{41}, N_{44} and N_{47}) and has a distorted octahedral geometry with N_{14} and N_{44} occupying the axial positions and N_1, N_{47}, N_{20} and N_{41} in the equatorial plane. Both tridentate dppt and dien are coordinated to Ru(II) atom in a meridional style.

Two phenyl rings in dppt are rotated away from the 1,2,4-triazine ring with dihedral angles (61.5° and 28.3°, respectively), however, the triazine ring is almost co-planar with the phenanthroline fragment in dppt according to the torsion angle (171.6°) of N14-C13-C15-N16. The mean distance of Ru-N(dppt) is 2.03 Å, comparable to that of $[Ru(dppt)(bpy)Cl]ClO_4$ (2.0549 Å) [35], and the mean Ru-N (dien) distance is 2.113 Å. Although the shortest Ru-N (dppt) is from the central ring of dppt [Ru(1)-N(14), 1.945(4) Å] rather than the terminal ones [Ru-N(1), 2.141(4) and Ru-N(20), 2.003(3) Å], the shortest Ru-N (dien) is connected with the terminal nitrogen (N47) rather than the middle one (N44) of dien, similar to what occurs in Pt dien complex [36].

3.2. *DNA-binding properties*

3.2.1. Electronic absorption titration. In order to compare the DNA-binding strength between the dien conplexes and dipn ones and discuss the effect of features of co-ligand aliphatic polyamine on DNA-binding properties, the data of UV absorption titration with DNA and the DNA-binding constants K'_{b1} based on Wolf's equation [37] for **1** and **2** were calculated and listed in table S2 (Supporting Information). On one hand, the appearing hypochromisms at MLCT transition bands (figure 2) of both **1** and **2** (7.60 and 16.07, respectively) resulting from the addition of DNA suggest that the two complexes interact with DNA most likely through a mode that involves a stacking interaction between the aromatic chomophore and the base pairs of DNA; the differences in the hypochromism (**2** is much greater than **1**, and these two complexes are less than those of the related dipn-containing complexes: $[Ru(dppt)(dipn)]^{2+}$ > **1**, and $[Ru(pta)(dipn)]^{2+}$ > **2**) indicate that **2** has a bigger DNA-binding affinity than **1**, and that the dipn complexes have larger DNA-binding constants than the corresponding dien complexes [19].

These DNA-binding results reflect that the plane of pta in **2** is favorable for deep insertion into the DNA double helix, and the non-coplanar two phenyl rings situated at the end of dppt is an obstruction to DNA intercalation for **1**. The differences in DNA-binding ability between the dien and dipn complex are likely explained by the differences in the ability of aliphatic polyamine to form hydrogen bonds for each complex. The greater the strength of the hydrogen bond formed

between the NH_2 or NH segment of the co-ligand and oxygen of water molecules (that mainly lie in the major groove of DNA [5, 6] and of the phosphate groups of the DNA), the bigger the deterrent to intercalation to DNA for the overall complex. Such H-bonds were reported to form in the DNA-binding process of $[Ru(NH_3)_4(dppz)]^{2+}$ [17] and the 1,4,8,11-tetraazacyclotetradecane Ru(II) complexes [38]. In this way, the dien complex has a smaller DNA-binding constant relative to the dipn complex because of its better hydrophilicity and more easily formed H-bond, in accord with the results of UV-titration experiment. The binding of **1** and **2** to DNA may be from the major groove, because this orientation is in favor of forming hydrogen bonds between dien and H_2O in the major groove [5, 6].

In order to further explain this DNA-binding trend of **1** and **2**, theoretical calculation was made using the density functional calculation (DFT) method (Supporting Information). The reported HOMO energy of the DNA section model are -0.047 atomic units [39], much higher than the energy of the LUMO or HOMO for **1** and **2** (table S2). Meanwhile, the "electronic cloud" of the HOMO in the DNA model is predominantly distributed on the base pairs of DNA, and that of the LUMO are mainly distributed on dppt and pta (figure S2). Such electron configurations can cause electron transition from the HOMO of DNA to the LUMO of the complexes, and the lower LUMO energy of the complex should be more advantageous to the DNA-binding of the complex in intercalation mode. From table S2, we can see the order: E_{LUMO}(**1**) > E_{LUMO}(**2**), E_{LUMO}(**1**) > E_{LUMO}($[Ru(dppt)(dipn)]^{2+}$), and E_{LUMO}(**2**) > E_{LUMO} ($[Ru(pta)(dipn)]^{2+}$), thus resulting in the DNA binding affinity order above.

3.2.2. Thermal denaturation studies. The DNA melting point T_m is the temperature at which half of the total base pairs are unbonded [40]. The melting curves of the absorption intensity at 260 nm of CT-DNA in the absence and presence of Ru(II) complexes versus temperature are given in figure 3. The observed change in melting temperatures (ΔT_m) at a concentration ratio [DNA]/[Ru] = 10:1 is 1.6 and 5.1 °C for **1** and **2**, respectively, which means the DNA became much more stable reacting with **2** than with **1**. Accordingly, it can be derived that **2** binds to DNA through

intercalation mode, like $[Ru(NH_3)_4dppz]^{2+}$ (ΔT_m = 5.2) [17], and that **1** may be in partial intercalation or electrostatic interaction, though this requires further confirmation via viscosity measurements below.

The MLCT absorptions are affected by the depth of intercalation of the aromatic chomophore (dppt or pta) in the base pair of DNA, due to the interaction of the DNA π stack and the drug π system. The magnitudes of the hypochromism of the MLCT absorption bands depend on the strength of the intercalative interaction [41].

Differential scanning calorimetry (DSC) is a useful method for determining the DNA-binding constant at the DNA melting temperature, the enthalpy of DNA melting, and the DNA-binding enthalpy of reagents binding to helical base pairs [28, 42]. Here, based on the data obtained in UV titration and thermal denaturation experiments, and the enthalpy of DNA melting (ΔH_m = 28.9 kJ·mol^{-1} bp) obtained from DSC [42], we can calculate a complete thermodynamic profile of the DNA binding of **1** and **2** with application of McGhee's and van't Hoffs equations [27, 29]; all the calculated values are listed in table 3. The binding of the complexes to DNA is energetically favorable at room temperature (according to the negative ΔG^o and ΔH^o values), which is in accord with the results of DFT calculation mentioned above. Meanwhile, the negative ΔH^o and ΔG^o values demonstrate that the hydrogen bond between the N-H of co-ligand dien and the O (from DNA's sugar-phosphate backbone and the water molecules in the major groove), as well as the stacking interaction between the DNA bases and the intercalative or semi-intercalative ligand dppt or pta, have ascendancy over hydrophobic interaction – as seen in the reported results of the calorimetric and equilibrium DNA-binding study [43].

3.2.3. Viscosity measurements. The viscosity of a DNA solution is sensitive to DNA-binding of the metal complexes, and the difference in binding mode leads to variance in pattern of DNA viscosity changes. A classical intercalation results in lengthening of the DNA helix, as base pairs are separated to accommodate the binding agents, leading to increase in DNA viscosity; a partial intercalation mode could bend (or kink) the DNA helix, reduce its effective length and,

concomitantly, its viscosity. This was used as the basis for our further confirming the binding mode of the present complexes [28].

The results of viscosity measurements for **1** and **2** are shown in figure 4. The relative viscosity of DNA decreases with increasing concentrations of **1**. However, when the concentration of **2** is increased the relative viscosity of DNA increases steadily. Thus, by inference, the two complexes could bind to DNA in two different modes with **2** binding in a classical intercalation and **1** in a partial intercalation, in agreement with the results obtained from the electronic absorption titration and thermal denaturation studies above.

On the basis of these experiments, the binding constants of **1** and **2** and other analogue Ru(II) complexes with ammonia or amine as ancillary ligand are smaller than those of aromatic polypyridine (as ancillary ligand) complexes [17-20, 44].

3.3. *Photocleavage of pBR 322 DNA by Ru(II) complexes*

An agarose gel electrophoresis experiment is a useful method for investigating the photocleavage of pBR322 DNA induced by small molecules, because the moving rates for three types of circular plasmid DNA are different. The intact supercoiled form I is the fastest, the nicked Form II with one cleaved strand is the slowest, and the linear Form III with both strands cleaved is between Form I and Form II [45].

The results of photocleavage of pBR 322 DNA by Ru(II) complexes (figure 5) showed that no obvious cleavage was observed when DNA alone was subjected to irradiation for 30 minutes at 365 nm (line 1), or when DNA was mixed with the complexes in darkness for 30 minutes (lines 2 and 6); the cleavage of pBR322 DNA only happened under the combination of binding to a complex and irradiating at 365 nm, and the amount of Form I and Form II diminished or increased gradually with increasing concentrations of **1** or **2**, respectively. This result also revealed that the cleavage of pBR322 DNA triggered by **1** and **2** took place through single-strand scission.

3.4. *Antioxidant activity studies*

Reactive oxygen species (ROS) are ubiquitous as part of normal cellular metabolism and defense systems. At appropriate concentrations, they play important roles in the regulation of cellular growth, differentiation, proliferation, and apoptosis, whereas at high levels they can bring about deleterious effects on organisms, even causing various diseases such as cancer, ischemia, atherosclerosis, diabetes, Alzheimer's disease, *etc*. [46]. The hydroxyl radical (•OH), usually generated by Fenton or Fenton-like reactions, especially at low concentrations of "low"-valent transition metal complexes, is the most reactive ROS and can induce mutagenicity and carcinogenicity at excessively high concentrations *in vivo* [47, 48]. Thus, it is important to find certain antioxidants that can scavenge these excess ROS, especially the hydroxyl radical, from a living body [49]. To date, many natural and synthesized materials have been reported as scavengers of •OH, such as lycopene [50], curcumin [51], polyphenol [52] and rare earth [53] or ruthenium coordination compounds [7, 49]. Many methods have also been designed to measure the antioxidant activity of the •OH scavengers *in vitro* [32, 54, 55].

In order to explore the possible abilities of the two Ru-polyamine complexes in scavenging •OH, two steps were taken: the antioxidant activity was determined by measuring the bleach of absorbance of safranin resulting from the reactions of **1** and **2** with the literature method [7, 32]; the change in the amount of •OH with respect to an increase in the supply of Ru(II) complexes was determined by monitoring the absorbance intensity of safranin, which could be photo-bleached upon its reaction with •OH. This allows the antioxidant activity against the hydroxyl radical for **1** and **2** to be known. The bar diagram representation of the scavenging ratio, taken as $(A_i-A_0)/(A_c-A_0) \times 100\%$ versus the concentrations of **1** and **2**, is presented in figure 6. The suppression of •OH by **1** and **2** reached 83.3% and 77.7% at 10 μM of Ru(II) complexes, respectively. The two Ru(II) complexes show efficient antioxidant activity against the hydroxyl radical, and the scavenging ratio of **1** is much higher than that of **2** under the same experimental conditions. The •OH suppression strength order is contrary to the DNA-binding strength order for the two complexes; this is similar to the

case of complexes $[Ru(dmb)_2(dcdppz)]^{2+}$ and $[Ru(bpy)_2(dcdppz)]^{2+}$ (dmb = 4,4'-dimethyl-2,2'-bipyridine, dcdppz = h,j-dichlorodipyrido[3,2-a:2',3'-c]phenazine) [7e].

Although, the •OH scavenging properties of Ru(II) complexes are important for their utilities as antioxidants, we should note that, according to the reported papers [56, 57], the assays of detecting the hydroxyl radical scavenging properties of some antioxidant *in vitro* are not biologically relevant, and the antioxidants added to living samples inhibit oxidative stress not directly by scavenging hydroxyl radicals. Here, the Ru(II) complexes **1** and **2**, if as antioxidants *in vivo*, may react with the less reactive $RO_2\cdot$ (relative to the •OH) in biological systems, concomitantly shorten or terminate the radical chain processes. This is probably responsible for the indirect scavenging of ROS [58]; the detailed mechanism needs to be further researched.

3.5. *Cell viability assay*

The cell viability was evaluated by MTT [34]. The cell viability results obtained after incubating with **1** and **2** at different concentrations from 1 to 200 μM against BEL-7402 (hepatocellular), HELA (human cervical carcinoma), and A549 (human pulmonary carcinoma) are illustrated in figure 7. The inhibitory concentration 50 (IC_{50}) is defined as the concentration required to reduce the size of the cell population by 50%. The IC_{50} values of **1** and **2** against the three selected tumor cell lines are listed in table 4. The toxicities of the complexes were concentration dependent, namely, the cell viability decreased with increasing complex concentration. Although higher complex concentration reduced the percentages of cell survival, there is a significant difference in susceptibility between **1** and **2**. It can be concluded that the greater the strength of the DNA-binding, the greater the toxicity against cancer cells for **1** and **2**. It is also noticed that, for some electrostatic DNA-binding Ru(II) complexes with ammonium groups, the greater the strength of the DNA-binding, the lesser the toxicity against cancer cells, implying that DNA-binding mode can inflect cytotoxicity of Ru(II) complexes [59].

4. Conclusion

A combination of absorption titration, thermal denaturation, and viscosity measurement demonstrates that the DNA-binding affinity of **2** is greater than that of **1**, and that **2** binds to CT-DNA in an intercalative mode but **1** binds to it in partial intercalation. Meanwhile, the reaction of the complexes with DNA is an energy-driven process with a decrease of entropy, and the hydrogen binding between the N-H of co-ligand dien and N or O on the bases of the sugar-phosphate backbone of DNA, as well as the stacking interaction between the DNA bases and the intercalative or semi-intercalative ligand dppt or pta, are more important than hydrophobic interaction. The cleavage of pBR322 DNA triggered by **1** and **2** takes place through single-strand scission and is a Ru(II) complex concentration-dependent process. The results of the cell viability assay indicate that the greater the strength of DNA-binding, the greater the toxicity against cancer cells for **1** and **2**. However, the scavenging activity has no bearing upon the DNA-binding ability, according to the results in scavenger measurements.

Acknowledgements

This work was supported by the National Science Foundation of China (No. 21071099), the National Science Foundation of Guangdong Province (No. 2014A030307015), the Featured Innovation in Colleges and Universities of Guangdong Province (Natural Science) Project (2014) and Shaoguan University. We are grateful to Prof. Hui Chao (Sun Yat-Sen University) for his specific directions and Prof. Kang-Cheng Zheng (Sun Yat-sen University) for the good work on the DFT calculation.

Supporting information available: CCDC 943190 crystallographic data for this paper can be obtained free of charge from the Cambridge Crystallographic Data Centre via www.ccdc.cam.ac.uk/data_request/cif. The DFT calculation can be obtained free of charge via the Internet at http://www.tandfonline.com.

References

[1] S.R. Rajski, R.M. Williams. *Chem. Rev*., **98**, 2723 (1998).

[2] (a) L.N. Ji, X.H. Zou, J.G. Liu. *Coord. Chem. Rev*., **216-217**, 513 (2001). (b) S. Shi, J. Liu, K.C. Zheng, C.P. Tan, L.M. Chen, L.N. Ji. *Dalton Trans*., 2038 (2005). (c) H. Chao, F. Gao, L.N. Ji. *Prog. Chem*., **19**, 1844 (2007). (d) L.M. Chen, J. Liu, J.C. Chen, S. Shi, C.P. Tan, K.C. Zheng, L.N. Ji. *J. Mol. Struct*., **881**, 156 (2008). (e) F. Gao, X. Chen, J.Q. Wang, Y. Chen, H. Chao, L.N. Ji. *Inorg. Chem*., **48**, 5599 (2009). (f) B. Sun, J.X. Guan, L. Xu, B.L. Yu, L. Jiang, J.F. Kou, L. Wang, X.D. Ding, H. Chao, L.N. Ji. *Inorg. Chem*., **48**, 4637 (2009). (g) H.J. Yu, S.M. Huang, L.Y. Li, H.N. Jia, H. Chao, Z.W. Mao, J.Z. Liu, L.N. Ji. *J. Inorg. Biochem*., **103**, 881 (2009). (h) X. Chen, F. Gao, Z.X. Zhou, W.Y. Yang, L.T. Guo, L.N. Ji. *J. Inorg. Biochem*., **104**, 576 (2010). (i) X. Chen, J.H. Wu, Y.W. Lai, R. Zhao, H. Chao, L.N. Ji. *Dalton Trans*., **42**, 4386 (2013). (j) H.Y. Huang, P.Y. Zhang, B.L. Yu, Y. Chen, J.Q. Wang, L.N. Ji, H. Chao. *J. Med. Chem*., **57**, 8971 (2014).

[3] Y. Liu, R. Hammitt, D.A. Lutterman, L.E. Joyce, R.P. Thummel, C. Turro. *Inorg. Chem*., **48**, 375 (2009).

[4] H. Song, J.T. Kaiser, J.K. Barton. *Nature Chem*., **4**, 615 (2012).

[5] H. Niyazi, J.P. Hall, K. O'Sullivan, G. Winter, T. Sorensen, J.M. Kelly, C.J. Cardin. *Nature Chem*., **4**, 621 (2012).

[6] J.P. Hall, K. O'Sullivan, A. Naseer, J.A. Smith, J.M. Kelly, C.J. Cardin. *PNAS*, **43**, 17610 (2011).

[7] (a) Y.J. Liu, Z.H. Liang, Z.Z. Li, C.H. Zeng, J.H. Yao, H.L. Huang, F.H. Wu. *BioMetals*, **23**, 739 (2010). (b) H.L. Huang, Y.J. Liu, C.H. Zeng, L.X. He, F.H. Wu. *DNA Cell Biol*., **29**, 261 (2010). (c) Y.J. Liu, Z.H. Liang, Z.Z. Li, J.H. Yao, H.L. Huang. *J. Organomet. Chem*., **696**, 2728 (2011). (d) G.B. Jiang, Y.Y. Xie, G.J. Lin, H.L. Huang, Z.H. Liang, Y.J. Liu. *J. Photochem. Photobiol., B*, **129**, 48 (2013). (e) B.J. Han, G.B. Jiang, J.H. Yao, W. Li, J. Wang, H.L. Huang, Y.J. Liu. *Spectrochim. Acta, Part A*, **135**, 840 (2015).

[8] U. Schatzschneider, J. Niesel, I. Ott, R. Gust, H. Alborzinia, S. Wolfl. *ChemMedChem*., **3**, 1104 (2008).

[9] M.R. Gill, J.A. Thomas. *Chem. Soc. Rev*., **41**, 3179 (2012).

[10] J. Liu, W.J. Zheng, S. Shi, C.P. Tan, J.C. Chen, K.C. Zheng, L.N. Ji. *J. Inorg. Biochem*., **102**, 193 (2008).

[11] C. Qian, J.Q. Wang, C.L. Song, L.L. Wang, L.N. Ji, H. Chao. *Metallomics*, **5**, 844 (2013).

[12] Y.Y. Xie, H.L. Huang, J.H. Yao, G.J. Lin, G.B. Jiang. *Eur. J. Med. Chem*., **63**, 603 (2013).

[13] T.F. Chen, Y.N. Liu, W.J. Zheng, J. Liu, Y.S. Wong. *Inorg. Chem*., **49**, 6366 (2010).

[14] C.A. Puckett, J.K. Barton. *J. Am. Chem. Soc*., **129**, 46 (2007).

[15] L.Y. Li, H.N. Jia, H.J. Yu, K.J. Du, Q.T. Lin, K.Q. Qiu, H. Chao, L.N. Ji. *J. Inorg. Biochem*., **113**, 31 (2012).

[16] E. Wang, C.M. Giandomenico. *Chem. Rev*., **99**, 2451 (1999).

[17] R.B. Nair, E.S. Teng, H.L. Kirkland, C.J. Murphy. *Inorg. Chem*., **37**, 139 (1998).

[18] P.U. Maheswari, M. Palaniandavar. *Inorg. Chim. Acta*, **357**, 901 (2004).

[19] X.L. Hong, H. Chao, L.J. Lin, K.C. Zheng, H. Li, X.L. Wang, F.C. Yun, L.N. Ji. *Helv. Chim. Acta*, **87**, 1180 (2004).

[20] X.L. Hong, H. Chao, J.H. Yao, H. Li, L.N. Ji. *Polyhedron*, **23**, 815 (2004).

[21] J. Marmur. *J. Mol. Biol*., **3**, 208 (1961).

[22] M.E. Reichmann, S.A. Rice, C.A. Thomas, P. Doty. *J. Am. Chem. Soc*., **76**, 3047 (1954).

[23] R.H. Blessing. *Acta Cryst. A*, **51**, 33 (1995).

[24] Bruker AXS, Madison, WI, *SHELXTL* 5.1 (1991).

[25] G.M. Sheldrick, Göttingen University, Germany SHELX 97 (1997).

[26] M.T. Carter, M. Rodriguez, A.J. Bard. *J. Am. Chem. Soc*., **111**, 8901 (1989).

[27] J.D. McGhee. *Biopolymers*, **15**, 1345 (1976).

[28] (a) S. Satyanarayana, J.C. Dabrowiak, J.B. Chaires. *Biochemistry*, **32**, 2573 (1993). (b) S. Satyanarayana, J.C. Dabrowiak, J.B. Chaires. *Biochemistry*, **31**, 9319 (1992).

[29] H.Q. Liu, B.C. Tzeng, Y.S. You, S.M. Peng, H.L. Chan, M.S. Yang, C.M. Che. *Inorg. Chem.*, **41**, 3161 (2002).

[30] J.B. Chaires, N. Dattagupta, D.M. Crothers. *Biochemistry*, **21**, 3933 (1982).

[31] G. Cohen, H. Eisenberg. *Biopolymers*, **8**, 45 (1969).

[32] W.H. Koppenol. *Free Rad. Biol. Med.*, **15**, 645 (1993).

[33] C.C. Winterbourn. *Biochem. J.*, **198**, 125 (1981).

[34] T. Mosmann. *J. Immunol. Methods*, **65**, 55 (1983).

[35] X.L. Hong, H. Chao, C.S. Xi, X.L. Wang, L.N. Ji. *Anal. Sci. (The Japan Soc. Anal. Chem.)*, **20**, x49-50 (2004).

[36] M.W. Ndinguri, F.R. Fronczek, P.A. Marzilli, W.E. Crowea, R.P. Hammer, L.G. Marzilli. *Inorg. Chim. Acta*, **363**, 1796 (2010).

[37] A. Wolf, G.H. Shimer Jr., T. Meehan. *Biochemistry*, **26**, 6392 (1987).

[38] H.L. Chan, H.Q. Liu, B.C. Tzeng, Y.S. You, S.M. Peng, M. Yang, C.M. Che. *Inorg. Chem.*, **41**, 3161 (2002).

[39] N. Kurita, K. Kobayashi. *Comput. Chem.*, **24**, 351 (2000).

[40] J.M. Kelly, A.B. Tossi, D.J. McConnell, C. OhUigin. *Nucleic Acids Res.*, **13**, 6017 (1985).

[41] A.M. Pyle, J.P. Rehmann, R. Meshoyrer, C.V. Kumar, N.J. Turro, J.K. Barton. *J. Am. Chem. Soc.*, **111**, 3051 (1989).

[42] F. Leng, J.B. Chaires, M.J. Waring. *Nucleic Acids Res.*, **31**, 6191 (2003).

[43] I. Haq, P. Lincoln, D. Suh, B. Norden, B.Z. Chowdhry, J.B. Chaires. *J. Am. Chem. Soc.*, **117**, 4788 (1995).

[44] M. Shilpa, C.S. Devi, P. Nagababu, J.N.L. Latha, R. Pallela, V.R. Janapala, K. Aravind, S. Satyanarayana. *J. Coord. Chem.*, **66**, 1661 (2013).

[45] J.K. Barton, A.L. Raphael. *J. Am. Chem. Soc.*, **106**, 2466 (1984).

[46] I. Olmez, H. Ozyurt. *Neurochem. Int.*, **60**, 208 (2012).

[47] S. Goldstein, D. Meyerstein, G. Czapski. *Free Radical Biol. Med.*, **15**, 435 (1993).

[48] S. Rachmilovich-Calis, A. Masarwa, N. Meyerstein, D. Meyerstein, R. van Eldik. *Chem. Eur. J.*, **15**, 8303 (2009).

[49] B. Lipinski. *Oxid. Med. Cell Longev.*, **2011**, 1 (2011).

[50] A.K. Prasad, P.C. Mishra. *J. Mol. Model.*, **20**, 2233 (2014).

[51] E. Kunchandy, M.N.A. Rao. *Int. J. Pharm.*, **58**, 237 (1990).

[52] N.R. Perron, J.L. Brumaghim. *Cell Biochem. Biophys.*, **53**, 75 (2009).

[53] T.R. Li, Z.Y. Yang, B.D. Wang, D.D. Qin. *Eur. J. Med. Chem.*, **43**, 1688 (2008).

[54] I.P. Kaur, T. Geetha. *Mini-Rev. Med. Chem.*, **6**, 305 (2006).

[55] N. Udilova, A.V. Kozlov, W. Bieberschulte, K. Frei, K. Ehrenberger, H. Nohl. *Biochem. Pharm.*, **65**, 59 (2003).

[56] D. Meyerstein. *J. Coord. Chem.*, **66**, 2076 (2013).

[57] D. Meyerstein. *Isr. J. Chem.*, **54**, 279 (2014).

[58] S. Selvamurugan, P. Viswanathamurthi, A. Endo, T. Hashimoto, K. Natarajan. *J. Coord. Chem.*, **66**, 4052 (2013).

[59] J. Sun, W.X. Chen, X.D. Song, X.H. Zhao, A.Q. Ma, J.X. Chen. *J. Coord. Chem.*, **68**, 308 (2015).

Figure captions

Figure 1. An ORTEP drawing of $[Ru(dppt)(dien)]^{2+}$ (50% probability level ellipsoids).

Figure 2. Absorption spectra of **1** (a) and **2** (b) in Tris-HCl buffer upon addition of CT-DNA ([Ru] = 20 μM, [DNA] = 0-160 μM). The arrows indicate the changes in absorbance upon increasing the DNA concentration. Inset: plot of $(\varepsilon_a - \varepsilon_f) / (\varepsilon_b - \varepsilon_f)$ versus [DNA] for the titration of DNA to Ru(II) complex.

Figure 3. Melting temperature curves of DNA in the absence and presence of the complexes, [Ru] = 10 $\mu mol \cdot L^{-1}$, [DNA] = 100 $\mu mol \cdot L^{-1}$.

Figure 4. Effect of increasing amounts of the complexes on the relative viscosities of DNA at 30.0±0.1 °C ([DNA] = 0.5 mM and [Ru]/[DNA] = 0.00, 0.02, 0.04, 0.06, 0.08, 0.10, 0.12).

Figure 5. Photoactivated cleavage of pBR 322 DNA in the presence of different concentrations of Ru(II) complex after irradiation at 365 nm for 30 min.

Figure 6. Scavenging effect of **1** and **2** on hydroxyl radicals. Experiments were performed in triplicate.

Figure 7. Cell viability of **1** and **2** on tumor BEL-7402 (a), A549 (b) and HELA (c), cell proliferation *in vitro*. Each data point is the means ± standard error obtained from at least three independent experiment.

Journal of Coordination Chemistry

Table 1. Crystal data and structural refinement for $[Ru(dppt)(dien)](ClO_4)_2$.

Empirical formula	$C_{31}H_{30}Cl_2N_8O_8Ru$
Formula weight	814.60
Temperature	100(2) K
Wavelength	0.71073 Å
Crystal system, space group	Monoclinic, P2(1)/n
Unit cell dimensions	a = 8.3407(17) Å α = 90° b = 28.122(6) Å β = 99.98(3)° c = 14.145(3) Å γ = 90°
Volume	3267.7(11) Å^3
Z, Calculated density	4, 1.656 Mg/m^3
Absorption coefficient	0.709 mm^{-1}
F(000)	1656
Crystal size	0.40 × 0.15 × 0.05 mm^3
θ range for data collection	1.45 to 25.00°
Index ranges	$-9 \leqslant h \leqslant 9$, $-33 \leqslant k \leqslant 33$, $-15 \leqslant l \leqslant 16$
Reflections collected / unique	36771 / 5656 [R(int) = 0.0462]
Completeness to θ = 25.00°	98.5%
Refinement method	Full-matrix least-squares on F^2
Data / restraints / parameters	5656 / 0 / 448
Goodness-of-fit on F^2	1.020
Final R indices [I>2σ(I)]	R_1 = 0.0476, wR_2 = 0.1016
R indices (all data)	R_1 = 0.0778, wR_2 = 0.1096
Largest diff. peak and hole	1.090 and -0.784 e·Å^{-3}

Table 2. Selected bond lengths (Å) and angles (°) for X-ray structural segment of $[Ru(dppt)(dien)]^{2+}$.

Ru(1)-N(1)	2.141(4)	Ru(1)-N(14)	1.945(4)
Ru(1)-N(20)	2.003(3)	Ru(1)-N(41)	2.116(4)
Ru(1)-N(44)	2.110(3)	Ru(1)-N(47)	2.109(4)
N(14)-Ru(1)-N(20)	78.69(14)	N(20)-Ru(1)-N(41)	92.94(14)
N(14)-Ru(1)-N(47)	98.00(14)	N(47)-Ru(1)-N(41)	162.45(13)
N(20)-Ru(1)-N(47)	94.93(14)	N(44)-Ru(1)-N(41)	81.72(14)
N(14)-Ru(1)-N(44)	175.30(14)	N(14)-Ru(1)-N(1)	79.28(14)
N(20)-Ru(1)-N(44)	96.64(14)	N(20)-Ru(1)-N(1)	157.91(14)
N(47)-Ru(1)-N(44)	81.81(14)	N(47)-Ru(1)-N(1)	89.71(14)
N(14)-Ru(1)-N(41)	98.91(14)	N(44)-Ru(1)-N(1)	105.40(14)
N(41)-Ru(1)-N(1)	88.87(14)		

Journal of Coordination Chemistry

Table 3. Thermodynamic parameters based on UV DNA melting experiment.

	1	**2**
T_m (°C)	75.3	78.8
ΔT_m (°C)	1.6	5.1
K_{b2} (M^{-1})	7.8×10^3	3.3×10^4
K_{b1} (M^{-1})	5.5×10^4 (s = 1.6)	7.4×10^5 (s = 1.9)
$\Delta G°$ ($kJ \cdot mol^{-1}$)	-27.0	-33.5
$\Delta H°$ ($kJ \cdot mol^{-1}$)	-33.5	-50.7
$\Delta S°$ ($J \cdot mol^{-1} \cdot K^{-1}$)	-21.6	-57.6

The T^0_m (the T_m of DNA alone) was 73.6 °C, the T_m of CT-DNA in the presence of Ru(II) complex in a 10:1 ratio of base pair to complex, and the value of standard free energy change was set at 25 °C.

Table 4. The IC_{50} values of **1** and **2** against selected cell lines.

Compound	IC_{50} (μM)		
	BEL-7402	A549	HELA
1	>200	>200	>200
2	>200	23.69 ± 3.35	106.68 ± 5.78

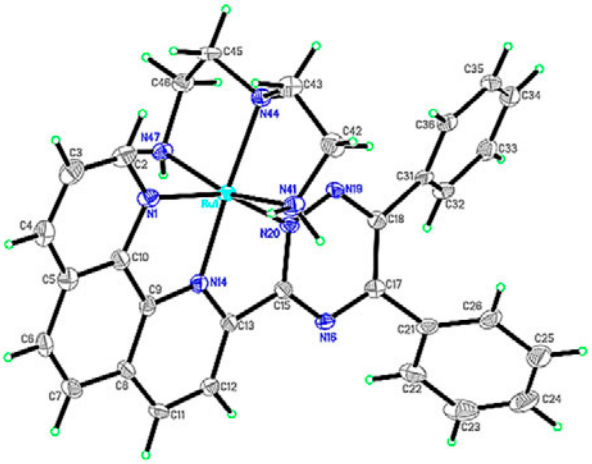

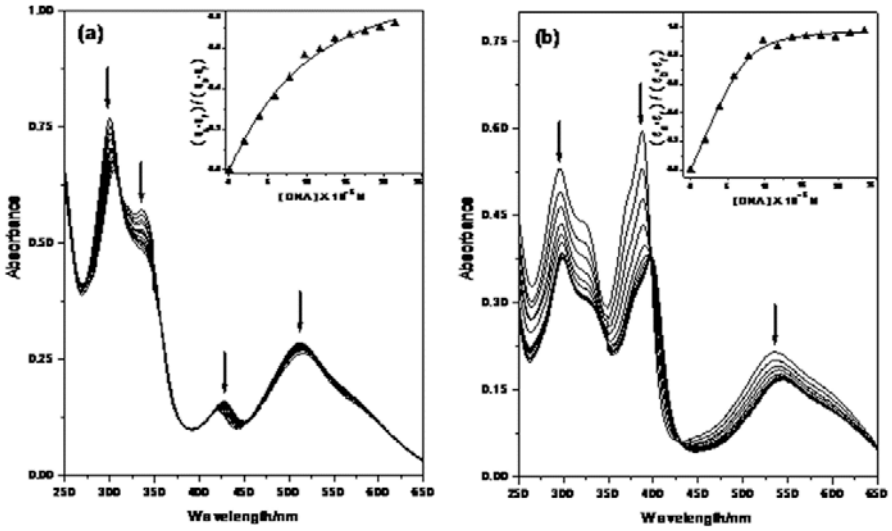

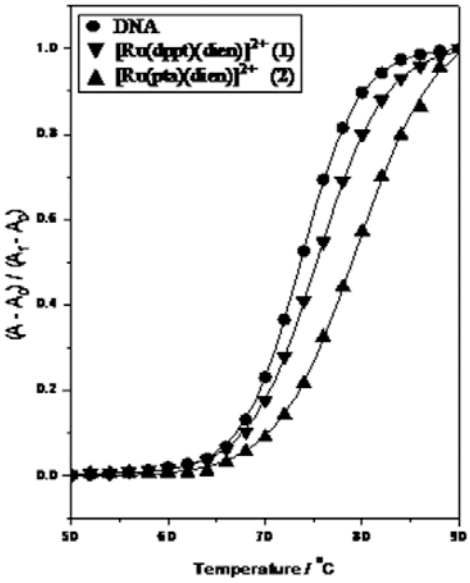

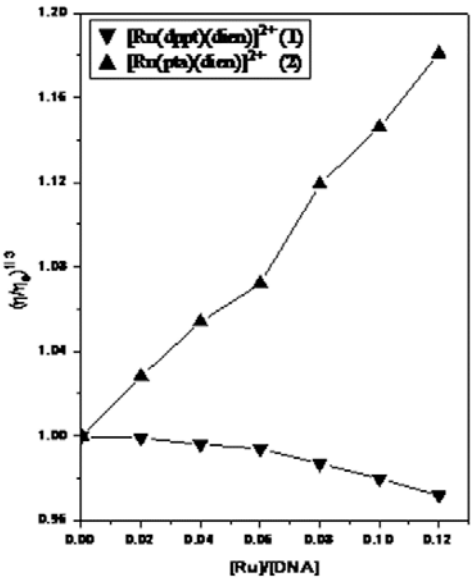

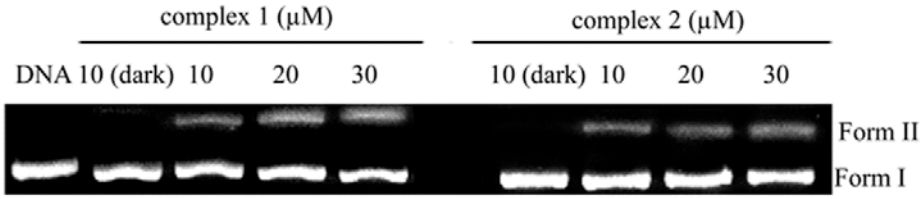

Journal of Coordination Chemistry